JOURNAL OF MATERIALS SCIENCE 27 (1992) 4009–4015

Dynamic observations of Sn–Pb solder reflow in a hot-stage environmental scanning electron microscope

H. S. BETRABET, J. K. McKINLAY, S. M. McGEE
Department of Materials Engineering and Characterization, Philips Laboratories, Briarcliff Manor, NY 10510, USA

Solidification behaviour of solders has a critical effect on the resulting microstructures and hence mechanical properties. Therefore, it is essential to understand the effects of soldering processing parameters on microstructure to engineer optimum microstructures. Microstructural changes in the solder that occur during the reflow process were studied in a hot-stage environmental scanning electron microscope (ESEM). An off-eutectic Sn60–Pb40 solder and a dispersion-strengthened solder with the same Sn–Pb ratio were reflowed in an ESEM, and changes in the microstructure were recorded on video tape. The dissolution and nucleation of grains during melting and solidification were observed. It was found that the microstructure of the conventional solder became coarser when it was allowed to solidify from a melt where the proeutectic lead was not completely dissolved. Grain refinement was observed in dispersion-strengthened solder where the dispersoids acted as heterogeneous nucleation sites.

1. Introduction

Sn–Pb alloys are the most often used solder materials in the microelectronics industry for the interconnection of components to substrates. The expanded use of surface-mount technology has increased the importance of the mechanical properties of solders. This is because, in addition to providing electrical contacts, the solders function as structural members by mechanically supporting surface-mounted devices on circuit boards. Mechanical properties of the alloys such as strength, ductility, and resistance to fatigue failures are governed by their microstructures. Additionally, alloys of this type exhibit unstable microstructures in that they tend to coarsen at operating temperatures. It has been demonstrated that there is a direct correlation between thermal fatigue cracking and coarsened microstructures [1–3]. Therefore, it is essential to understand the effect of soldering processing parameters on microstructure to engineer the most favourable microstructures.

Most soldering processes involve a reflow step during which the solder melts and re-solidifies. The mechanical properties and reliability of the solder joints are strongly influenced by the reflow step. From static experiments, it is well known that higher cooling rates during solidification result in finer grain size solder leading to higher strength, increased ductility, and longer fatigue life [4]. Other factors such as composition and the addition of particulate nuclei can also affect grain size and can be manipulated for that purpose. To examine and develop such control, it can be especially convenient to study the microstructural evolution during the reflow process. The hot-stage environmental scanning electron microscope (ESEM) [5, 6] is ideally suited for this.

Dynamic observations of solidification processes are difficult to carry out in conventional scanning electron microscopes (CSEM) because the secondary electron (SE) and back-scattered electron (BSE) detectors are sensitive to contamination and outgassing from the samples. Such experiments are now possible in the recently developed ESEM which is designed to allow the presence of gaseous environments in the specimen chamber. Pressure-limiting apertures and a differential pumping system keep the electron gun area under high vacuum (10^{-7} torr; 1 torr = 133.322 Pa) and contaminant-free, while allowing the pressure to increase progressively up to 20 torr in the specimen chamber.

The principles of image formation in the ESEM have been described in detail by Danilatos [7]. Because this is a relatively new commercially available technique, the image formation mechanism is briefly described. It is well known that the incident electron beam–specimen interactions give rise to several signals, which include SE, BSE, and X-rays [8]. The SE and BSE are normally used to form images in a CSEM. The SE detector used in CSEMs (Everhart Thornley Detector) uses an electric field to collect the secondary electrons. It can function only in high vacuum and cannot be used in gaseous atmospheres where gas breakdowns may occur. In the ESEM, the gas molecules themselves are used in the image-formation process. The SE collide with the gas molecules, ionize them and eject further secondary electrons. These SE are termed environmental second-

0022–2461

ary electrons (ESE), and they, in turn, can ionize additional gas molecules, causing a cascading effect. This process results in signal amplification. The environmental secondary electrons are detected by an environmental secondary electron detector which does not require the application of a strong electric field. The detector is placed in the final lens, coaxially with the microscope optical axis, giving it high collection efficiency and the ability to form images without shadowing effects. Detailed analyses of gas scattering and electron–gas molecule interactions have been reported by Danilatos [7].

In the present study, a solder composition most commonly used in the microelectronics industry, the off-eutectic Sn60–Pb40 solder, was reflowed in the ESEM. The dispersion-strengthened Sn60–Pb40 solder presently being developed was also reflowed in the ESEM under identical conditions. The dispersion-strengthened solder was produced by employing mechanical alloying techniques. Processing details and microstructures of dispersion strengthened solder are reported elsewhere [9].

Dynamic changes in the microstructure were recorded on a video tape in a VHS format video cassette recorder. Observations made during dissolution and nucleation of grains during the solder melting and solidification are discussed.

2. Experimental procedure

Solder preforms for reflow experiments were prepared by powder compaction of the conventional and dispersion-strengthened solder. Powder samples, 3 g each, were loaded in a 6.35 mm diameter die and pressed to a pressure of 700 mPa in a closed-loop servo-hydraulic press (MTS) to form rods. The compacted solder rods were upset pressed to a thickness of 2 mm and finally cold-rolled in a jeweller's rolling mill to form a sheet 0.7 mm thick.

Solder joints were prepared by reflowing the sheet between two copper blocks ($12.7 \times 6.35 \times 3.17\ mm^3$) on a hot plate at 220 °C, without flux. A flowing reducing-gas mixture ($95He–5H_2$) was used to prevent oxidation. Because flux was not used during the reflow operation, the copper blocks were pretinned with Sn60–Pb40 solder to aid wetting. The reflowed solder joints were placed on a copper block for solidification. The samples were cross-sectioned using a slow-speed diamond saw, and metallographically prepared by grinding and polishing. The specimens were cut to fit in a 5 mm diameter crucible in the ESEM.

The solder joints were placed in an electrical furnace consisting of an electrical coil surrounding the crucible in the ESEM, and the system was purged and filled with a reducing gas mixture consisting of $90Ar–10H_2$ at 5 torr pressure. The ESEM was operated at 25 keV. The crucible temperature was monitored and controlled during the experiments. There may have been a difference between the measured temperature and solder temperature due to thermal lag between the crucible and solder. This precluded the assignment of actual temperatures to the micrographs shown in Figs 2 and 3.

The solder joints were melted and solidified by manually increasing the temperature to 170 °C at a rate of approximately 5 °C min^{-1} and then further increasing it to 195 °C at approximately 1 °C min^{-1}. The temperature was maintained at 195 °C for 30 s after which the furnace was turned off. This process was repeated except that the hold time at 195 °C was increased to 180 s. The microstructural evolution during melting and solidification was recorded on the video tape recorder. All images were obtained at a magnification of × 1600. Still photographs showing the sequence of events were taken from the video tape and are shown later in Figs 2 and 3.

3. Results and discussion

3.1. Melting and solidification of the conventional Sn60–Pb40 solder

The Pb–Sn diagram (Fig. 1) shows that the Sn60–Pb40 composition is slightly hypo-eutectic (lead-rich side of phase diagram) with a melting range of 183–189 °C (according to convention, the phase diagram is represented alphabetically). Therefore, some primary α-Pb is still solid above the eutectic temperature (183 °C) and is expected to melt only above 189 °C. Figs 2a–h show the microstructural evolution in the solder as it is heated from 170 °C to 195 °C, and held at that temperature for 30 s (Fig. 2h), and allowed to cool (Figs 2i–k). The microstructural changes that occur during the second reflow when the solder was held at 195 °C for 180 s are shown in Fig. 2l–r. It is apparent from Fig. 2h that while the 30 s hold time during the first reflow was insufficient for the complete melting of the primary α-Pb, the 180 s hold time was sufficient to produce a completely molten alloy (Fig. 2o). The incomplete melting during the first reflow may be due to a possible thermal lag between the crucible (whose temperature was monitored) and the solder, or because the hold time was insufficient for the α-Pb to melt completely.

It is important to compare the grain-size difference of the solder after solidification from the incomplete melt to that solidified from a completely molten state

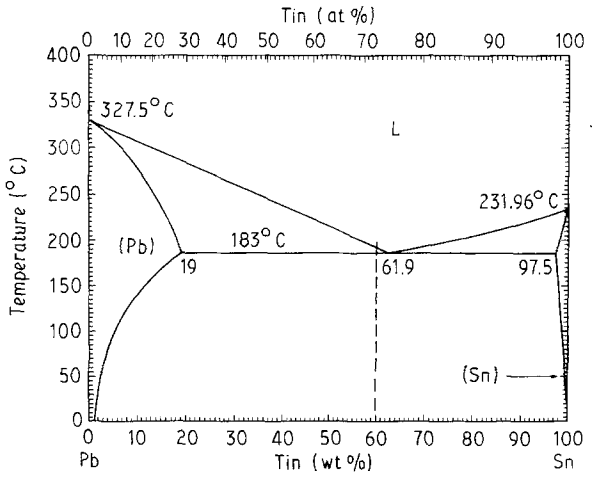

Figure 1 The Pb–Sn phase diagram showing the Sn60–Pb40 composition [17].

(Fig. 2k–r). The term "grain size" is used to refer to the size of the lead and tin phases in this discussion. The microstructure is clearly coarser when the solder is allowed to solidify before the primary α-Pb phase is completely molten. Therefore, to obtain finer microstructures, the Sn60–Pb40 solder should be maintained above the liquidus temperature at a sufficiently high temperature and time so that the primary α-Pb crystals are completely molten before the alloy is allowed to freeze.

The coarse microstructures obtained on solidification from incomplete melts can be explained based on observations made by several investigators during undercooling experiments [10–15]. Undercooling is defined as the difference between the liquidus temperature for a particular composition and the temperature at which recalescence begins to increase the specimen temperature. The latter temperature corresponds to the temperature at which the solidifying phase commences nucleation. The undercooling experiments have shown that the Pb–Sn system exhibits nonreciprocal nucleation. While the lead-rich phases act as poor nucleating agents for tin, the tin-rich phases provide potent nucleation sites for lead.

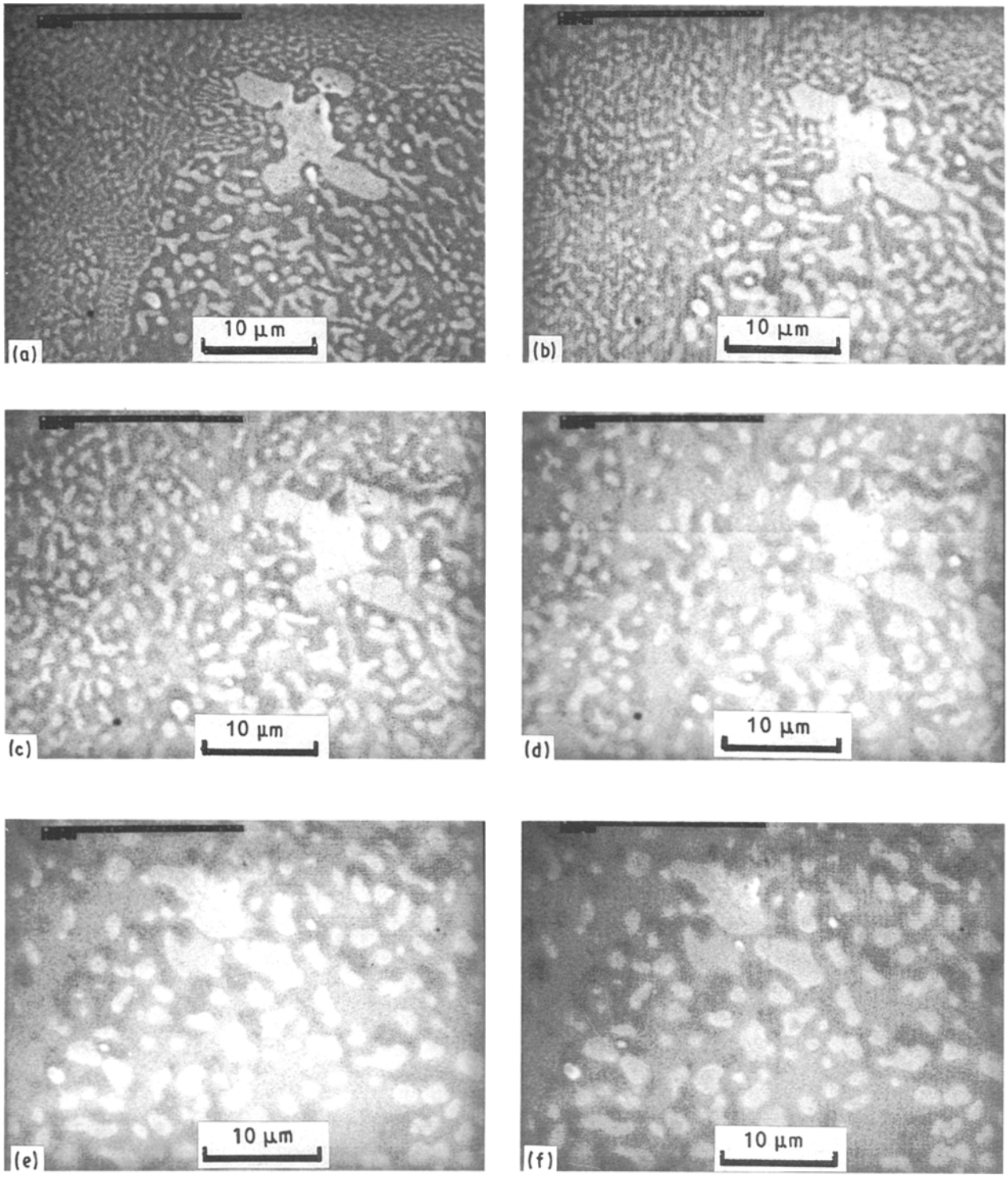

Figure 2 Microstructural evolution of conventional Sn60–Pb40 solder alloy during two reflow cycles. (a–h) Melting, (i–k) solidification during the first reflow cycle; (l–o) melting, (p–r) solidification during the second reflow cycle.

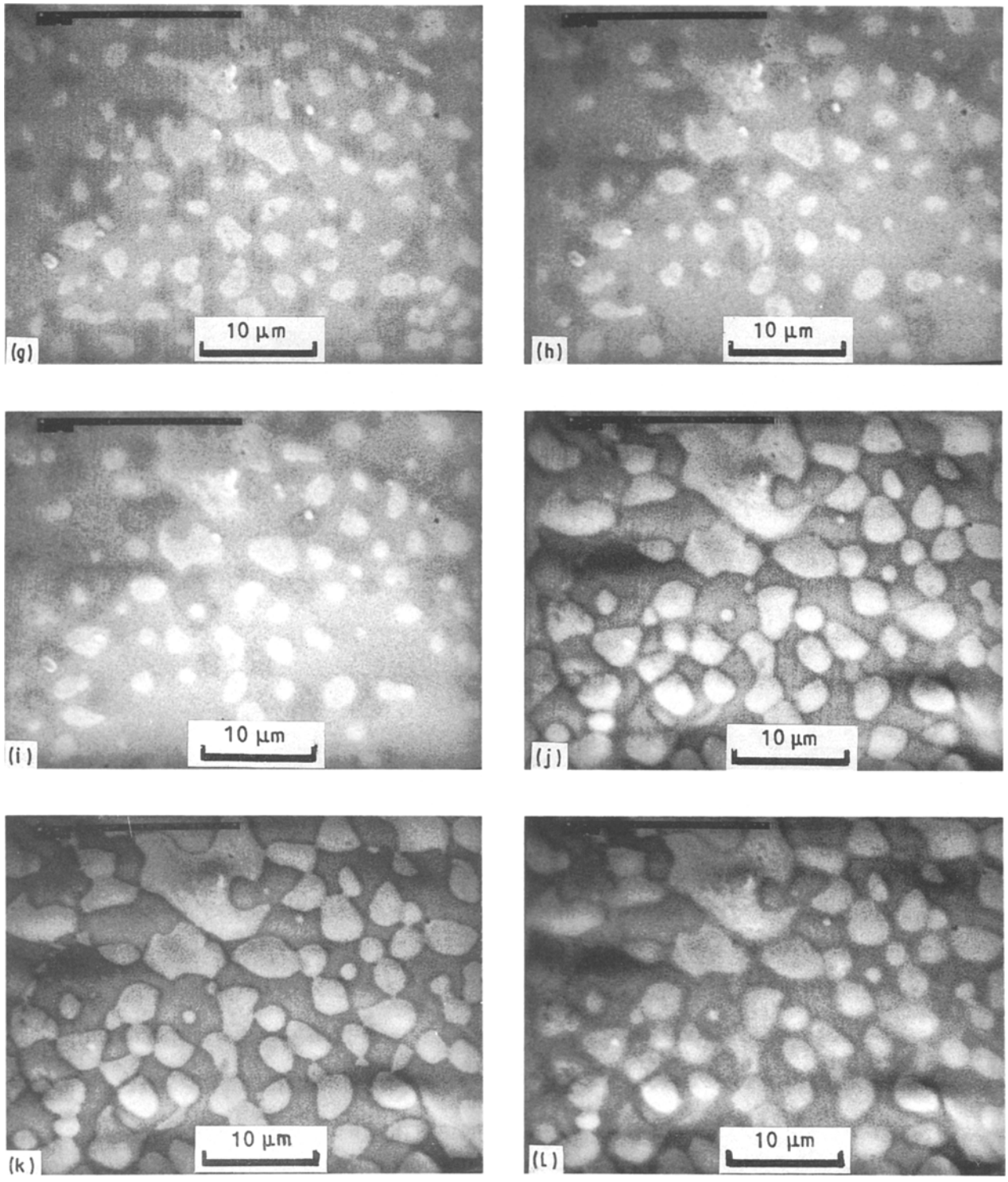

Figure 2 Continued.

According to Sundquist and Mondolfo [14], lead requires almost no undercooling in the presence of tin ($\Delta T = 0$–$0.5\,^{\circ}C$), whereas tin requires an undercooling of greater than 55 °C in the presence of lead. In fact, the undercooling required for nucleating lead heterogeneously on tin is similar to that for the homogeneous nucleation of lead. Chu *et al.* [13] have shown that the lead-rich phase nucleates before the tin-rich phase, even in hypereutectic compositions of up to 80 wt % Sn. Microstructural evidence for the non-reciprocal behaviour has been presented by deGroh and Laxmanan [11].

The non-reciprocal nucleation observed in the Pb–Sn system has been explained by Youdelis and Iyer [15] to be caused by differences in the distribution coefficients of the components. The component having the smaller distribution coefficient ($k_{Sn} = 0.066$) requires greater segregation of solvent and solute for growth than the component with the larger distribution coefficient ($k_{Pb} = 0.31$). Components with

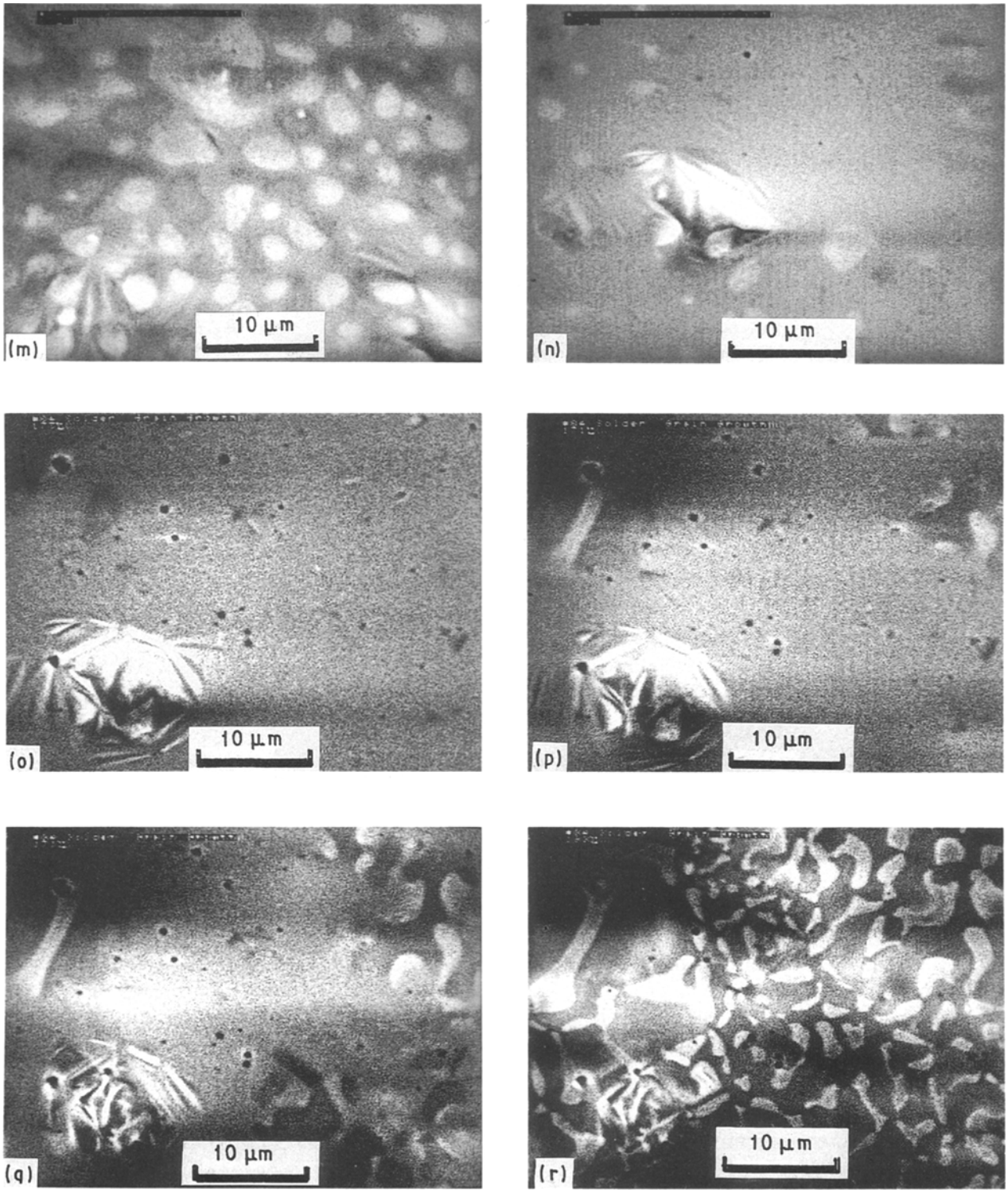

Figure 2 Continued.

smaller distribution coefficients need longer times for the transport processes diffusion and convection resulting in lower growth rates. Low growth rates cause a reduction in the rate of evolution of heat of fusion and, consequently, result in higher undercooling. Therefore, for hypoeutectic compositions in the Pb–Sn system, the primary α-Pb phase continues to grow while the tin phase is being undercooled, resulting in coarser microstructures. In our experiment, the unmelted primary α-Pb phases must have nucleated additional lead from the remaining liquid instead of tin, and further growth must have occurred while the tin was being undercooled.

Based on these observations, it would seem advantageous to use alloys which are hypereutectic rather than the hypoeutectic Sn60–Pb40 alloy to obtain finer microstructures. The primary tin phases will readily nucleate lead resulting in finer microstructures. However, for the tin-rich phase to nucleate before the lead-rich phase, the composition of the alloy would need to

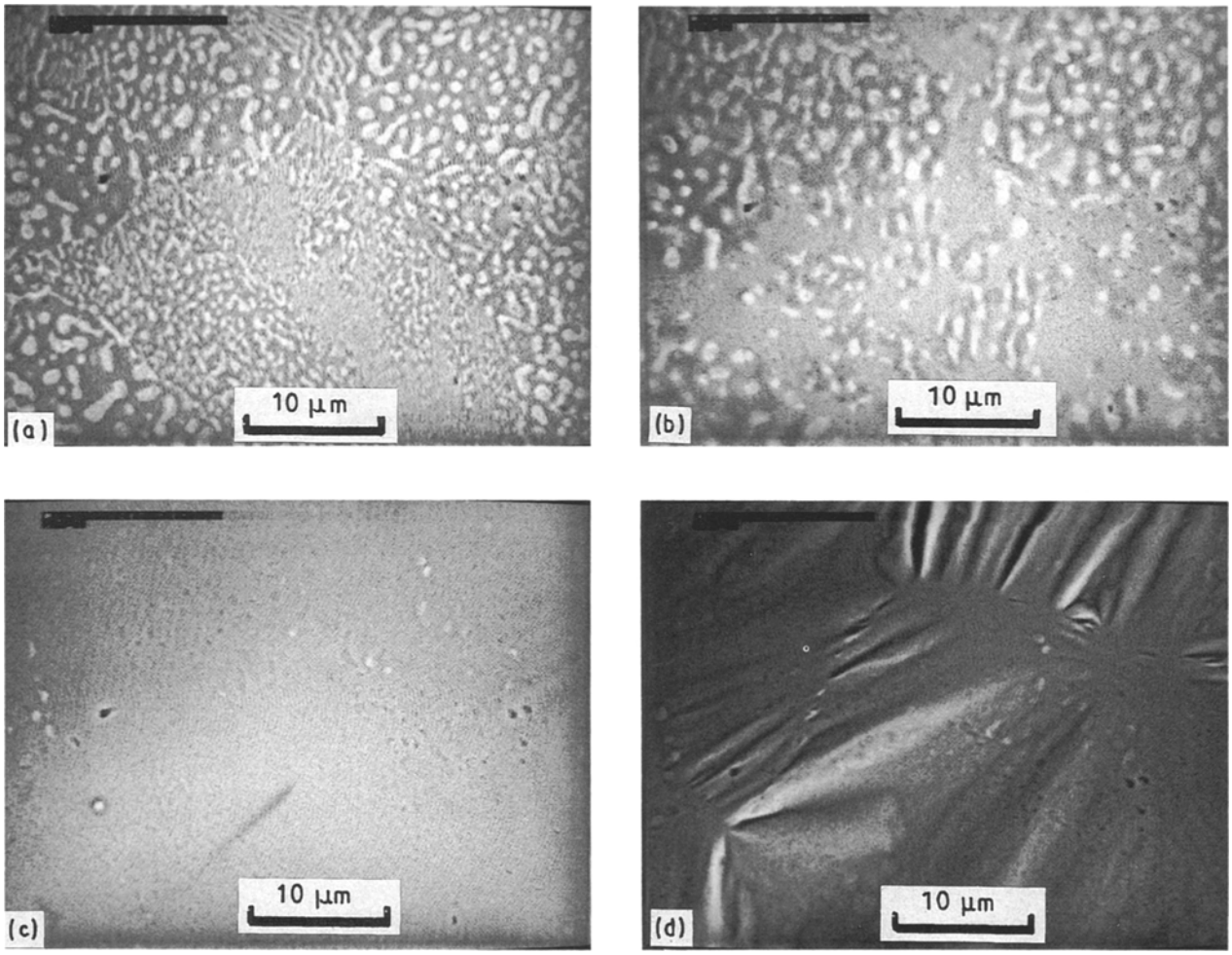

Figure 3 Microstructural evolution of dispersion-strengthened Sn60–Pb40 solder alloy during a reflow cycle. (a–d) Melting, (e–h) show solidification.

deviate substantially from the eutectic composition [11–13]. While the eutectic component of the resulting microstructure may have a fine grain size, massive tin dendrites are also present, as shown by deGroh and Laxmanan [11], thus precluding the use of such compositions.

3.2 Melting and solidification of the dispersion-strengthened solder

An alternative method for obtaining fine microstructures is to provide heterogeneous nucleation sites for the tin-rich phases by introducing appropriate particles into the solder. The resulting reduction in undercooling can be expected to result in finer microstructures, and in addition, reduce the amount of gravity-driven macrosegregation which causes the lead-rich dendrites to sink to the bottom and the tin-rich phases to rise to the top [11, 12, 16]. The approach of introducing heterogeneous nucleation sites has been recently attempted by employing dispersion-strengthening techniques to Sn60–Pb40 solders [9]. The dispersoids introduced in the solder have been shown to prevent coarsening and preserve the microstructure of the solder in the solid state.

Figs 3a–h show the microstructural changes occurring in the dispersion-strengthened solder as it undergoes melting and solidification. Notice that the microstructure of the dispersion-strengthened solder is finer than that of the conventional Sn60–Pb40 solder before melting (Fig. 3a versus Fig. 2a). The solder is actually undergoing a second reflow step as it was initially reflowed during joint fabrication. The solder is completely molten in Fig. 3c and the oxide from the solder has come to the surface and has formed a wrinkled skin on the liquid solder in Fig. 3d. The $90Ar-10H_2$ is not sufficiently reducing at the reflow temperature to reduce the oxide from the solder. It merely helps prevent the solder from becoming further oxidized during reflow. It is clear from the series of micrographs that the microstructure of the reflowed dispersion-strengthened solder (Fig. 3h) is finer than that of the reflowed conventional solder (Fig. 2r) suggesting that the dispersoids acted as heterogeneous nucleation sites during solidification. Because one consequence of dispersion strengthening is development of finer microstructures, such solders can be expected to resist thermal fatigue better than the conventional solders. The resistance of dispersion-strengthened solders to microstructural coarsening is reported elsewhere [9], and their mechanical characterization is presently underway.

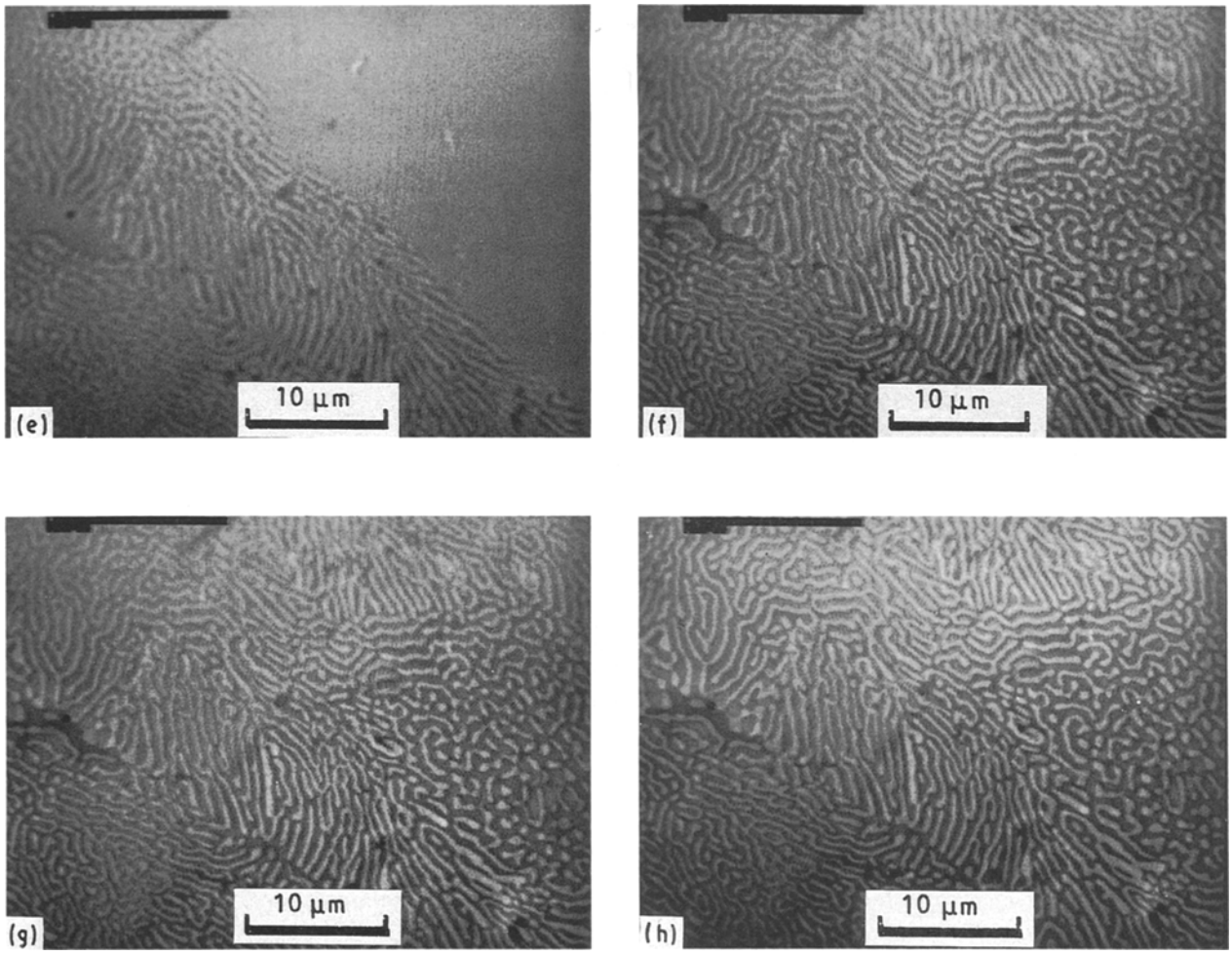

Figure 3 Continued.

4. Conclusions

1. The microstructure of conventional Sn60–Pb40 solder is coarser when the proeutectic lead is not completely dissolved prior to solidification.

2. The microstructure of the dispersion-strengthened solder is finer than that of the conventional solder upon solidification suggesting that the dispersoids act as heterogeneous nucleation sites.

3. *In situ* studies, such as solder reflow, can be routinely performed in the newly developed ESEM.

Acknowledgements

The authors thank Tom Hardt (Electroscan) for operating the ESEM and Doug Molloy for editing the video tape. A. Sicignano is thanked for suggesting the use of the ESEM for solder studies, and P. D. Goodell and R. H. Kane for helpful discussions.

References

1. D. FREAR, D. GRIVAS and J. W. MORRIS, *J. Metals* **40** (1988) 18.
2. *Idem, J. Electron. Mater.* **18** (1989) 671.
3. D. FREAR, *IEEE Trans. Comp. Hybrids Manf. Technol.* **13** (1990) 718.
4. J. F. ROEDER, M. R. NOTIS and H. J. FROST, in "Solder Mechanics, A State of the Art Assessment", edited by D. Frear, W. Jones and K. R. Kinsman (TMS, Warrendale, PA, 1991) p. 3.
5. N. BAUMGARTEN, *Amer. Lab.* June (1990).
6. *Idem, Nature* September (1989) 341.
7. G. D. DANILATOS, *Adv. Electron. Electron Phys.* **71** (1988) 109.
8. J. I. GOLDSTEIN, D. E. NEWBURY, P. ECHLIN, D. C. JOY, C. FIORI and E. LIFSHIN, in "Scanning Electron Microscopy and X-Ray Microanalysis" (Plenum, New York, 1981), p. 53.
9. H. S. BETRABET, S. McGEE and J. K. McKINLAY (1991) *Scripta Met. Mater.* **25** (1991) 2323.
10. J. H. HOLLOMAN and D. TURNBULL, *J. Metals* September (1951) 803.
11. H. C. deGROH III and V. LAXMANAN, *Metall. Trans.* **19A** (1988) 2651.
12. *Idem*, in "Solidification Processing of Eutectic Alloys", edited by D. M. Stefanescu, G. J. Abbaschian and R. J. Bayuzuck (TMS-AIME, Warrendale, PA, 1987) p. 229.
13. M. G. CHU, Y. SHIOHARA and M. C. FLEMINGS, *Metall. Trans.* **15A** (1984) 1303.
14. B. E. SUNDQUIST and L. F. MONDOLFO, *Trans. TMS-AIME* **221** (1961) 157.
15. W. V. YOUDELIS and S. P. IYER, *Met. Sci.* **9** (1975) 289.
16. L. WANG, V. LAXMANAN and J. F. WALLACE, *Metall. Trans.* **19A** (1988) 2687.
17. T. B. MASSALSKI, J. L. MURRAY, L. H. BENNETT and H. BAKER, in "Binary Alloy Phase Diagrams" (ASM, Metals Park, OH, 1986) p. 1848.

Received 22 April
and accepted 5 August 1991